Measurement: Sensors 38 (2025) 101718

Contents lists available at ScienceDirect

Measurement: Sensors

journal homepage: www.sciencedirect.com/journal/measurement-sensors

# Vibration measurement of wind turbine blades through image analysis of moiré pattern

ARTICLE INFO

*Keywords:*
Wind turbine blade
Vibration measurement
Moiré pattern analysis
Structural health monitoring

ABSTRACT

Wind turbine blades are becoming harder to maintain due to their growth in size in the last decade. Although the vibration of wind turbine blades can currently be monitored using sensors such as accelerometers or Fibre Bragg Grating sensors which are embedded on the blades, the maintenance work on the sensors themselves is also difficult. In this paper, a new and non-contact measurement method based on image analysis of moiré pattern is proposed to measure the out-of-plane vibration frequency of wind turbine blades. Experiments were conducted at different vibration frequencies and blade angles to verify the feasibility of the proposed method. Results show that in most conditions, the relative error of the measured frequency is within ±5 %. The proposed method is feasible on measuring vibration frequency of wind turbine blades resting at different angles.

## 1. Introduction

The wind energy sector has seen rapid growth in recent years, resulting in wind turbine manufacturers making ever larger wind turbines to improve energy output and efficiency. However, larger wind turbines come with larger structures, which increases the difficulty of operation and maintenance. Several metrics can be used to measure the structural health of wind turbine blades, one of which is its natural frequency. A change in natural frequency indicates a structural change in a wind turbine blade. A structural change can be cracks caused by fatigue, paint loss caused by lightning or corrosion, or weight and stiffness changes caused by ice accretion, which not only hinders the efficiency of the wind turbine but also causes catastrophic failure in the worst case.

The vibration frequency can be measured using several sensors. Currently, wind turbine blade vibrations are measured using a low-power wireless sensor network (WSN) embedded inside the blades [1]. Fibre Bragg Grating (FBG) sensors and strain gauges can be used to measure displacement as well as the frequency of a wind turbine blade [2]. However, FBGs need to be glued to the interior of the blade so it doesn't interfere with the airfoil. Even though contact sensors provide real-time information, they are difficult to be replaced or repaired once they are installed.

Non-contact measurement methods have been developed to measure vibration. Laser Doppler vibrometer (LDV), which measures the velocity of the blades, has also been used for measuring vibration velocity in several applications [3,4] and wind turbine blade vibrations [5,6]. Ozbek et al. compared the method of photogrammetry with the laser interferometry method and concluded that the laser interferometry method was only able to take measurements when the wind turbine was stationary, but photogrammetry could measure vibration displacements even during operation [5]. Unfortunately, photogrammetry requires accurate calibration of several cameras and synchronisation between them. This makes the measurement process difficult and time-consuming, which means it is not suitable to scale up for monitoring of the whole wind farm.

With advancements in image processing algorithms, image analysis-based methods have also been developed for non-contact measurement of vibration. Digital image correlation (DIC) is one of the methods that has gotten the most attention in the past decade [7]. It calculates the correlation between the two stereo cameras to achieve a sense of depth of field, which can then be converted into displacement of the vibrating object. A major advantage of DIC is that it can achieve similar accuracy as an LDV and is able to get full-field measurements. The biggest disadvantage with DIC is that the subject requires features to track. In the case of wind turbine blades, which have a white smooth surface, the surface has to be prepared with random dots to measure the full-field vibration [8] or markers aligned in a row to measure vibration at different locations [9]. On the other side of the spectrum, phase-based optical flow [10] does not require markers and simply uses phase-based motion magnification (PMM) [11] to amplify the motion and acquire vibration displacements. It has also been used to measure the vibration frequency as well as the mode shape of the blade. However, phase-based optical flow is only effective when the vibration is perpendicular to the camera. Vibrations can also be measured using moiré patterns. It is like a hybrid of the two methods mentioned above, having a marker that has gratings on it and uses image processing techniques to amplify and extract the vibration information. It has been used to measure the vibration of bridges [12].

In this paper, a new method based on analysis of moiré pattern is proposed to measure the flapwise vibration frequency of wind turbine blades with a camera perpendicular to the vibrating motion. It does not require camera calibration thus making it more suitable to deploy onto drones for autonomous inspection in wind farms. Furthermore, the amplification of the moiré pattern means that it can measure subtle vibrations from afar, making it much safer to operate. Since the proposed method only uses a single camera, it also eliminates the need for synchronisation and high-speed cameras. Unlike previous methods [12],

https://doi.org/10.1016/j.measen.2024.101718

Available online 30 December 2024

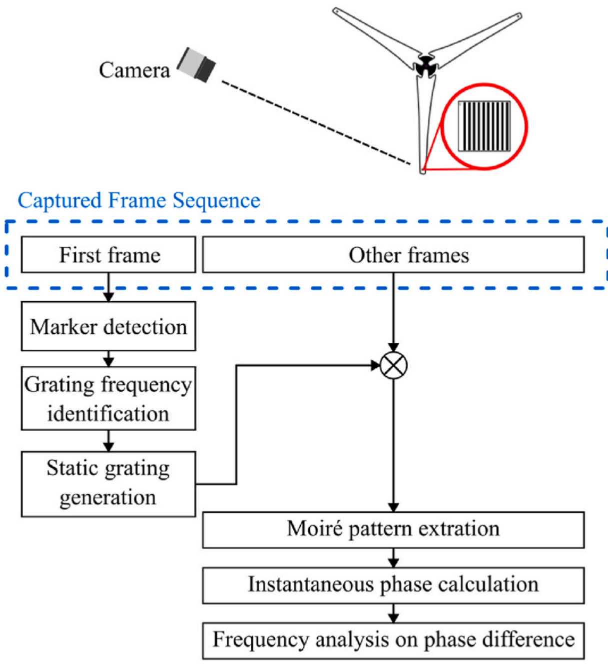


**Fig. 1.** System overview and flowchart of the image processing method.

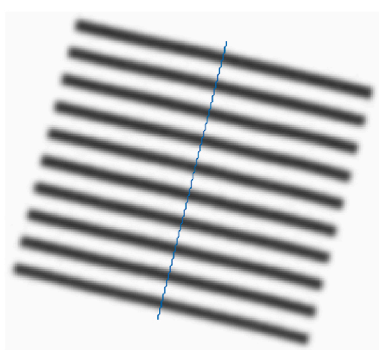

**Fig. 2.** The sampled line in the marker.

the proposed method is aimed to measure out-of-plane vibrations with markers in arbitrary positions.

## 2. Methods and procedures

The system overview and the image processing method are shown in Fig. 1. A camera is oriented towards the blade and captures the images of the marker on the blade. The first frame is used as a reference and processed following three major steps. First, the location of the grating pattern is detected, which provides the region of interest (ROI) for the moiré pattern analysis. Second, the frequency of the grating pattern is calculated. This is used in the next step to determine the generated grating frequency. The third and last step is to generate a static grating, which is superimposed on consecutive frames to induce the moiré pattern.

### *2.1. Marker detection and grating frequency identification*

Before any operation, the frames are converted to grayscale and smoothed. The grating pattern can be found by applying a local gradient filter to the grayscale image followed by Otsu thresholding. To be more specific, the gradient filter calculates the difference between the maximum and the minimum grey levels based on the structural element mask. Using a gradient filter ensures rotation invariance and some degree of scale invariance, which means that it will work with different grating orientations and camera distances. After segmentation, the grating orientation is calculated by finding its minimum bounding rectangle. Then, two centre lines are computed using the bounding rectangle. The reason for using the centre line is that the marker grating is designed to be symmetric at the centre. That means one of the centre lines will always be fully white. Hence, the correct cross-section can be selected by calculating its variance. The line of pixels sampled is shown in Fig. 2 and is analysed in the frequency domain to determine the dominant frequency, which is the grating frequency of the marker.

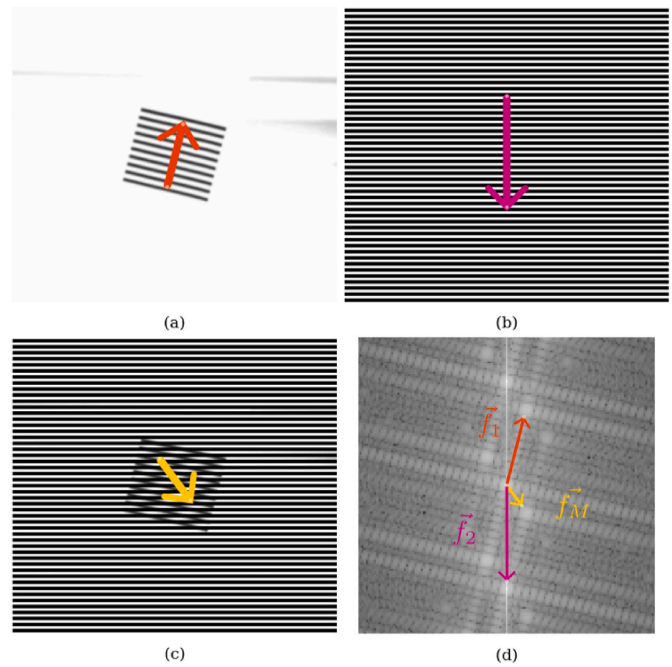


**Fig. 3.** Relationship between grating frequency vectors and the moiré pattern frequency vector. (a) Marker grating direction. (b) Generated static grating direction. (c) Moiré pattern direction. (d) Image spectrum of (c) showing all the components in the image.

### *2.2. Static grating generation*

According to Amidror [13], moiré patterns can be represented as spatial frequency vectors ($\vec{f}$), whose magnitude signifies the frequency of the grating and its angle shows the direction of travel. The moiré pattern happens when two or more frequency vectors are superimposed. Equation (1) shows the two-frequency vector case which is used in this paper.

$$\vec{f_M} = \vec{f_1} - \vec{f_2} \tag{1}$$

where $\vec{f_1}$ and $\vec{f_2}$ are spatial frequency vectors of gratings as illustrated in Fig. 3(a) and (b), respectively. $\vec{f_M}$ is the frequency vector of the moiré pattern as shown in Fig. 3 (c) generated by superimposing of the two gratings. The relationship between the two gratings and the moiré pattern is illustrated in Fig. 3 (d).

This equation can be simplified when both gratings are travelling in the same direction (i.e. the angle between $\vec{f_1}$ and $\vec{f_2}$ is 0° or 180°). Since spatial period (T) is the reciprocal of spatial frequency, the spatial period of the moiré pattern ($T_M$) can be written as shown in (2).

$$\frac{1}{T_M} = \left| \frac{1}{T_1} - \frac{1}{T_2} \right| \tag{2}$$

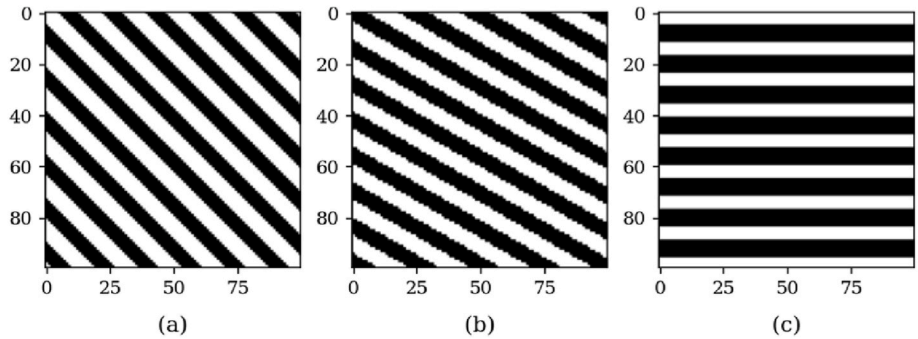


**Fig. 4.** Static grating with different angles, (a) 30, (b) 60, (c) 90.

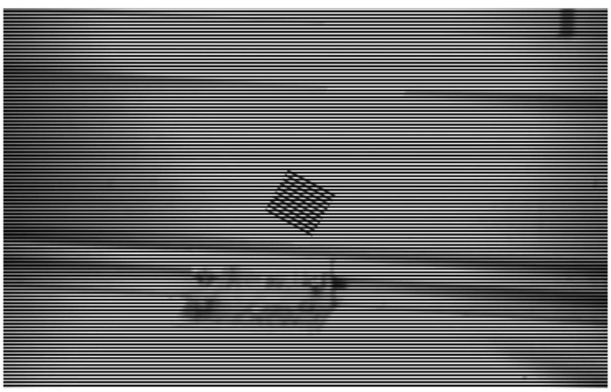

**Fig. 5.** Superimposed image between static grating and marker.

where $T_1$ and $T_2$ are the grating marker's spatial period and the generated static grating spatial period respectively. Equation (2) can be rewritten as a fraction between the moiré period and one of the grating periods as shown in (3).

$$\mu = \frac{T_M}{T_1} = \frac{1}{\left|1 - \frac{T_1}{T_2}\right|} \tag{3}$$

where μ is defined as the magnification factor. It can be easily seen that the closer the grating periods, the larger the magnification factor. Since the phase of the moiré pattern is directly influenced by the position of the gratings, the phase difference is also magnified.

The design of the static grating's spatial period ($T_2$) depends on the amount of magnification that should be applied to the original oscillation. Intuitively, it is possible to use the magnification factor directly as a design parameter and calculate the moiré pattern's spatial period thus getting a static grating period. This method, however, cannot guarantee the static grating's spatial period being an integer, which will result in the generated grating having uneven strips. This means that the grating period must be converted to an integer and the moiré period and magnification factor have to be recalculated. A better approach is to use the moiré period as a design parameter, which calculates the grating period from the moiré period and then the magnification factor. This approach makes it easy to find mistakes in the implementation, as it is easy to count the number of cycles in an image. The grating is generated using (4) taken from Ref. [14].

$$I_{ij} = 0.5 + 0.5\cos\left(\frac{2\pi N \times \left(x_i \cos\theta + y_j \sin\theta\right)}{T_2}\right) \tag{4}$$

where $I_{ij}$ is the grey level of pixel $(i, j)$ in an image with a width of N pixels and height of M pixels, θ is the angle at which the grating is travelling with respect to the x-axis, in our case it is always 90° since the grating is always travelling from the top of the image to the bottom of the image; $x_i \in Z : x_i \in [-N/2, N/2)$ , $y_j \in Z : y_j \in [-M/2, M/2)$ with $i = 1, 2, 3, \ldots, N$, $j = 1, 2, 3, \ldots, M$. Fig. 4 shows the generated gratings under different $\theta$ values.

The generated grating is superimposed onto the detected grating pattern, meaning that when the generated grating is less than or equal to 0.5, the resulting pixel is set to 0, when the generated grating is greater than 0.5, the resulting pixel will be the original grey level. The superimposed image is shown in Fig. 5.

### 2.3. Moiré pattern extraction and phase calculation

The superimposed image now contains the moiré pattern with a known period of ($T_M$). Unlike the theoretical approach which uses the orientation of $\overrightarrow{f_M}$, the orientation of $\overrightarrow{f_1}$ shown in Fig. 3 (a) is chosen to be analysed. This is because the grating's spatial frequency of the marker is determined by the rasterised sampled line, which has a different pixel scale when the marker is at various angles. To compensate for this, the static grating is always fixed at 90° and the orientation of $\overrightarrow{f_1}$ in the superimposed image will have the correct moiré period as designed using (2). The sampled line as shown in Fig. 2 is used again to extract the grey level from the superimposed image and the grey levels of the pixels on the sampled line constitute the composite signal in Fig. 6. Since the moiré period is already known, a simple bandpass filter can be used to filter on the composite signal and get the one-dimensional moire signal

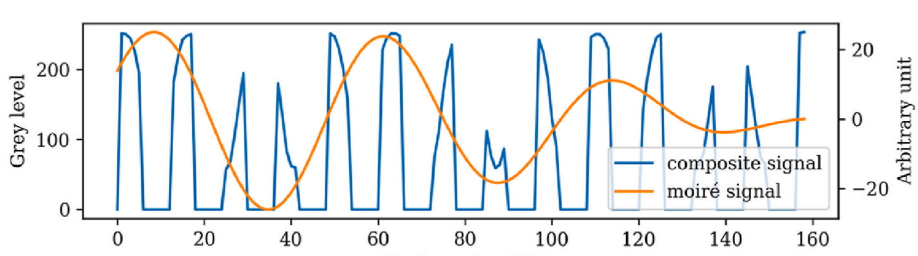


**Fig. 6.** Composited and extracted moiré pattern from a horizontal section of the image.

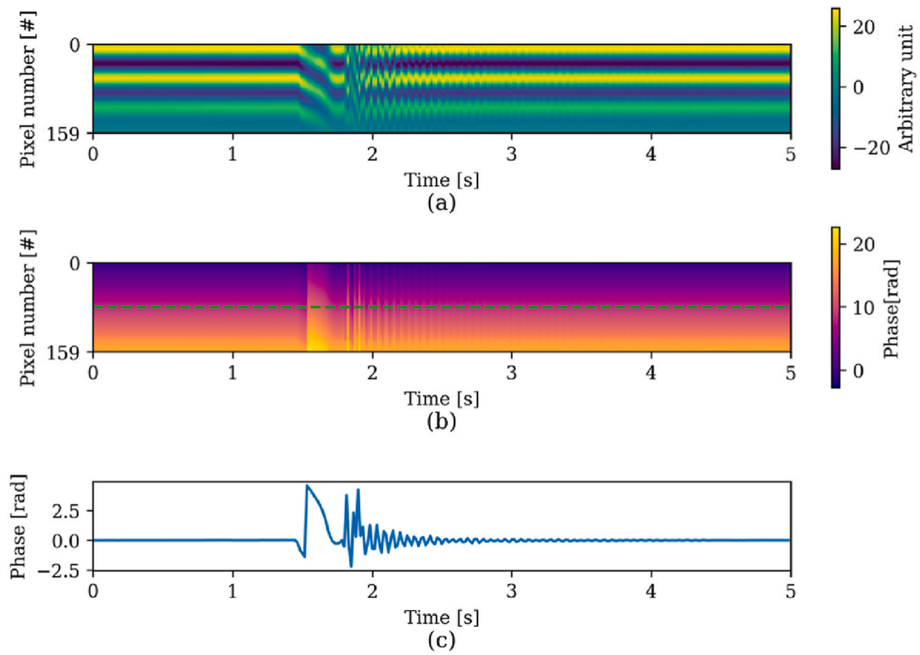


**Fig. 7.** (a) Moiré signals through time. (b) phases of the moiré signals after Hilbert transform. (c) Extracted phase from the centre of the marker (green dashed line).

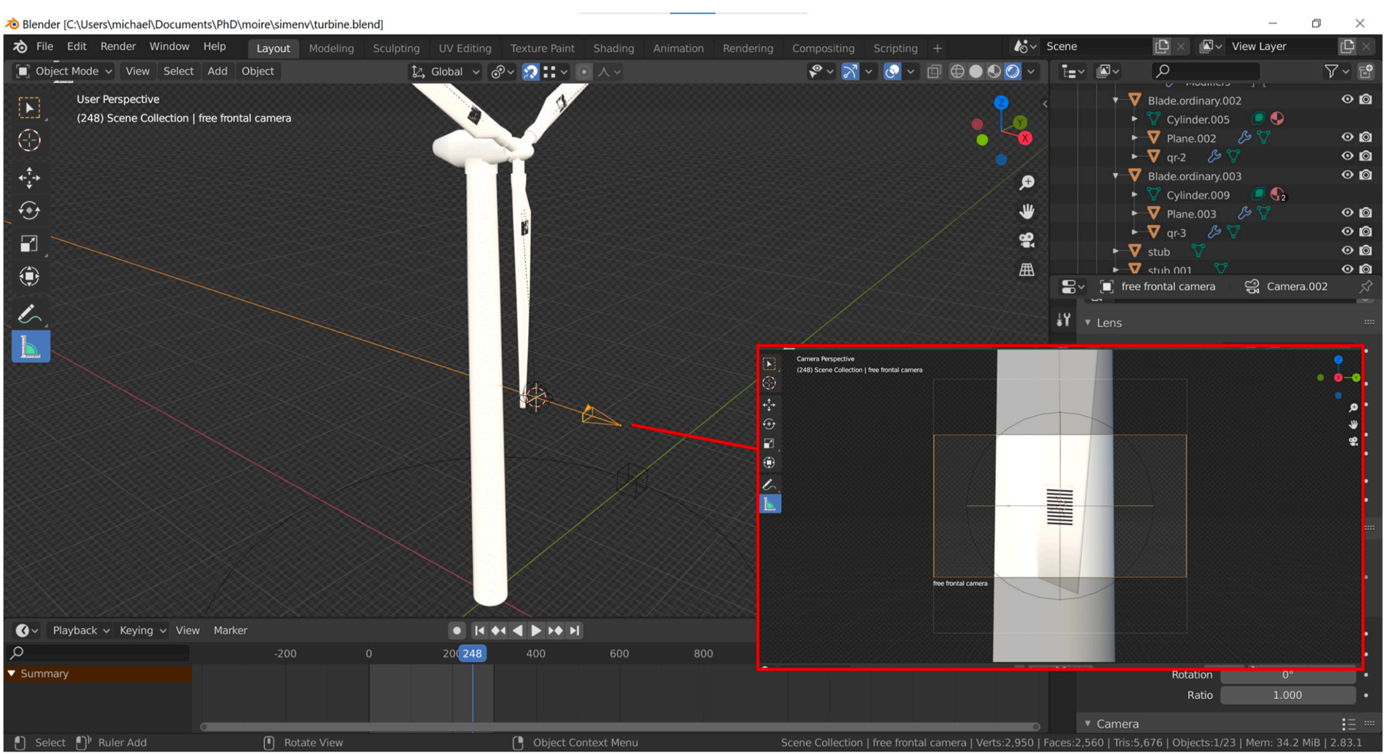


**Fig. 8.** Simulation environment in Blender.

shown in Fig. 6.

The moiré signal is computed for each frame and displayed with respect to time as shown in Fig. 7 (a). Through Hilbert transform, the phases of the signals in Fig. 7 (a) are calculated and shown in Fig. 7 (b). The phase on the green dash line in Fig. 7 (b) (the centre pixel on the marker) is extracted along the time axis and the phase difference between each frame and the first frame is calculated as shown in Fig. 7 (c). Since the phase difference reflects the motion of the vibration, the Fast Fourier Transform (FFT) can then be used to find the power spectrum of the vibration. The dominant peak of the spectrum will indicate the natural frequency at which the blade vibrates.

## 3. Experimental results and discussion

### 3.1. Simulation setup and results

A simulation model was built based on a real wind turbine – Nordtank NTK-300 in Blender is shown in Fig. 8. The camera is configured to

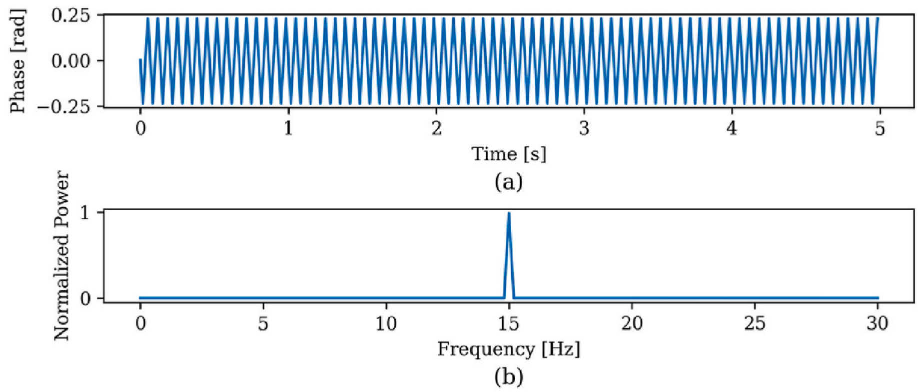


**Fig. 9.** Simulated 15 Hz vibration (a) Phase difference between each frame and the first frame (b) Power spectral density.

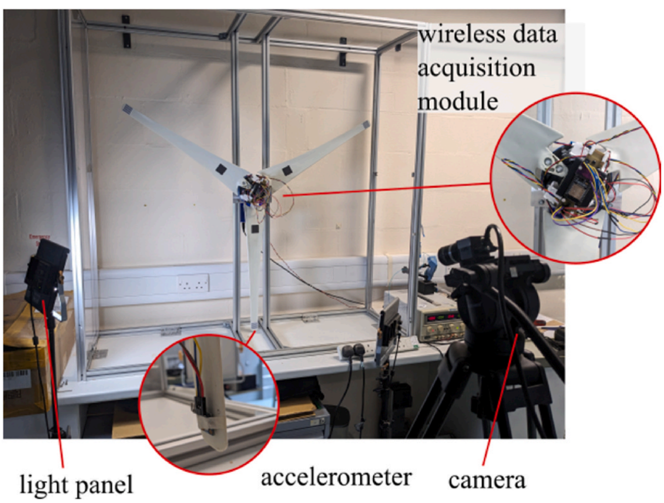


**Fig. 10.** Experimental setup of the wind turbine test rig.

have a 1/1.2” sensor paired with a 25 mm lens with the wind turbine blade pointing toward the ground. The images of the marker were obtained when the blade was vibrated at a frequency of 15 Hz. The simulation was used to validate the method and tests were later conducted on a small-scale wind turbine test rig.

The instantaneous phase of the moiré pattern is calculated and the phase difference between each frame and the first frame is obtained as shown in Fig. 9 (a). Through Fast Fourier transform (FFT), the power spectral density of the vibration is obtained as shown in Fig. 9 (b). Because the blade oscillation in the simulation model is configured without damping, the measured signal shows a uniform oscillation throughout the capture time. It can be seen that the proposed method was able to measure the vibration frequency of the blade with zero relative error under ideal conditions.

### 3.2. Experimental setup

Although simulations are able to validate the algorithm and have rudimentary motion blur and light conditions, it does not have the same properties as a real-world camera. In addition, unlike real blades, which have complex modes due to their complex structure, animated blades can only be configured to have a single-mode vibration. This is why measurements are moved to the wind turbine test rig shown in Fig. 10. The test rig is a modified commercial wind turbine with three blades that are 600 mm in length. To prevent the blades from moving, the stepper motor is engaged.

The camera (UEYE U3-3060CP-C-HQ Rev.2) mounted on the tripod has a gain of 70 % and an exposure of 13.34 ms. As typical vibration frequency of wind turbine blades is between 0.5 Hz and 30 Hz [15], the framerate of 60 fps is used in this study. The size of each frame is 1936 pixels × 1216 pixels. Additionally, the camera is paired with a 50 mm lens with an aperture of *f/2.8*. The light panel on the left is used to regulate the illuminance so it stays at 200 lux. Three accelerometers (MPU6050) are mounted at the tip of the blades on the back face to be used as the reference. The wireless data acquisition module based on an ESP32 is used to collect and transmit the accelerometer data to the computer via Bluetooth. Additional weight can be mounted on the blade to generate different vibration frequencies.

**Table 1**
Test matrix for experiments conducted on the wind turbine test rig.

| # | Weight position (mm) | Angle (°) |
|---|---|---|
| I | 0 | 0/15/30 |
| II | 0/250/300 | 0 |

Table 1 shows the test matrix of the experiments conducted on the test rig. In experiment I the blades were placed at three different locations with angles 0°, 15°, and 30°, where 0° means the wind turbine blade is pointing toward the ground and 15° and 30° are clockwise angles with respect to 0°. In experiment II, the weight is moved from the centre to different locations of the blade to imitate frequency changes on a faulty blade. For each condition, five different samples were taken, and the dominant frequency was located by finding the maximum power in the spectrum.

### 3.3. Experimental results and discussion

The proposed method is tested by taking measurements when the blade is situated at different angles. The measured phase shift is shown in Fig. 7 (c). It should be noted that the frequencies below 5.49 Hz is filtered to remove effects of edgewise vibration.

Fig. 11 shows the reference spectrum from the accelerometer and the measured spectrum from the proposed method at 0° (blade pointing toward the ground). It shows that at 0°, the vibration frequency from the accelerometer is 18.79 Hz. The measured vibration frequency is determined as 18.45 Hz which is the dominant frequency in the measured frequency spectrum, even though the oscillations caused by the broadband noise at the start of the test exist in the measured frequency spectrum.

The relative error between the vibration frequency measured by the accelerometer and that of the proposed method is shown in Fig. 12. The relative error ranges between −2.13 % and −1.97 % with all three angles having the same range.

The vibration frequency changes slightly when the weight is moved from the centre onto different positions of the blade. Tests are performed

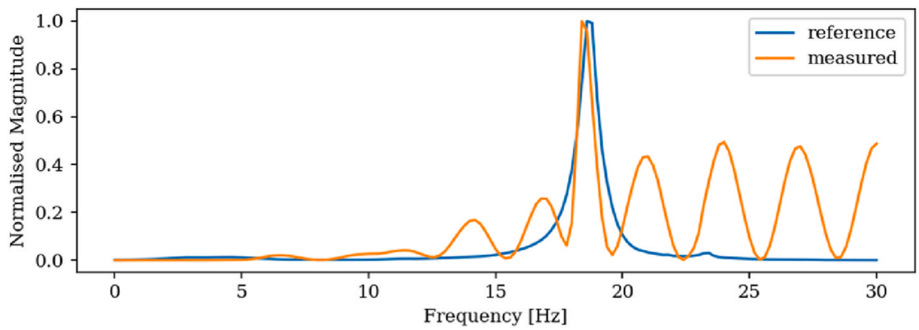


**Fig. 11.** Reference and measured vibration spectrum at 0°.

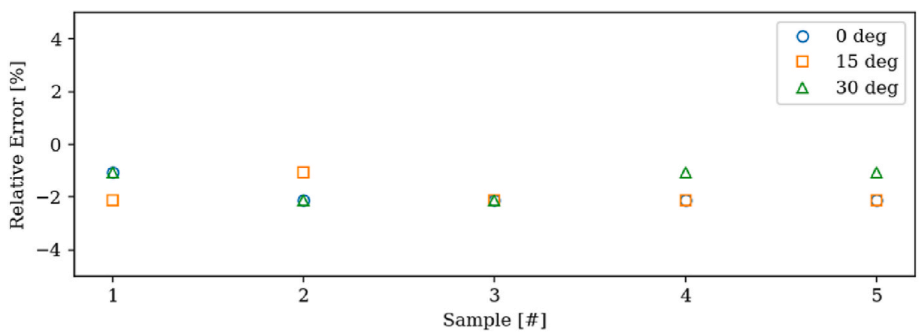


**Fig. 12.** Relative error of measured vibration frequency at different blade angles.

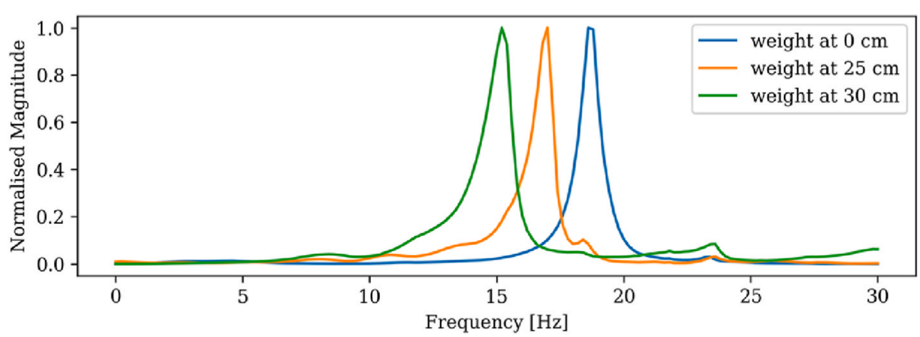


**Fig. 13.** Reference frequency spectrum when the weight is located at different positions of the blade.

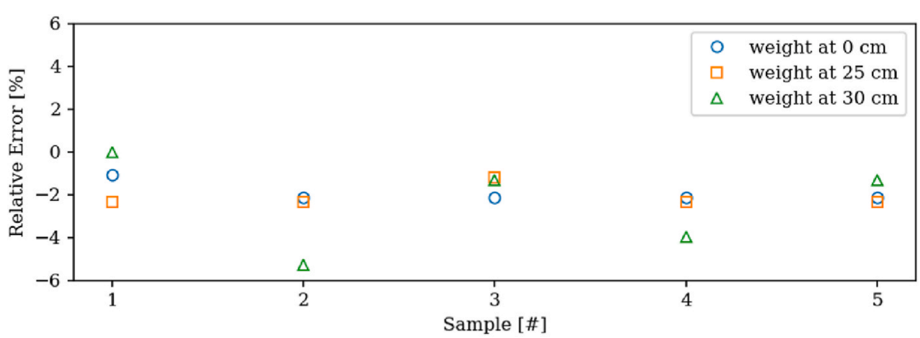


**Fig. 14.** Relative error of measured vibration frequency with different weight positions.

when the blade is resting at 0° and the wireless acquisition module is moved onto the blade at 25 cm and then moved to 30 cm. Fig. 13 shows the vibration frequency derived from the accelerometer measurements, which clearly shows a decrease in vibration frequency. When the weight is placed at 0 cm, 25 cm and 30 cm away from the centre, the vibration frequency is 18.76 Hz, 17.00 Hz and 15.20 Hz respectively.

The relative error of the measured vibration frequency at each condition is shown in Fig. 14. It can be seen that when the weight is located at 30 cm, it has the biggest relative error −5.23 %. During experimental tests, a few factors, such as camera configurations and environmental conditions, will affect the measurement accuracy. It is worth noting that the frame rate used in this paper is only 60 fps. By increasing frame rate, the measurement accuracy is expected to be improved further.

## 4. Conclusions

In this paper, a method based on moiré pattern analysis has been proposed to measure the vibration frequency of wind turbine blades. The proposed method was validated in a simulation environment and later tested on a wind turbine with blades at different angles to validate its rotation invariance. Moreover, external weight was added at different blade positions to assess its capability to measure different frequencies. The relative error is mostly around −2 % under laboratory conditions. Compared with the measurement tolerance of ±5 % used in Ref. [9], the proposed method is proven as a feasible way to measure the vibration frequency of wind turbine blades. In future, experimental tests for the measurement of vibration frequency and amplitude with blade in motion will be conducted. The effects of camera configuration and environmental conditions on the measurement accuracy will be systematically inverstaged to further improve the measurement system's performance.

## References

[1] R.A. Swartz, J.P. Lynch, S. Zerbst, B. Sweetman, R. Rolfes, Structural monitoring of wind turbines using wireless sensor networks, Smart Struct. Syst. 6 (3) (2010) 183–196, https://doi.org/10.12989/sss.2010.6.3.183.

[2] C.-H. Kim, I. Paek, N. Yoo, Monitoring of small wind turbine blade using FBG sensors, in: ICCAS 2010, Oct. 2010, pp. 1059–1061, https://doi.org/10.1109/ICCAS.2010.5669682.

[3] F. Dreier, P. Günther, T. Pfister, J.W. Czarske, A. Fischer, Interferometric sensor system for blade vibration measurements in turbomachine applications, IEEE Trans. Instrum. Meas. 62 (8) (Aug. 2013) 2297–2302, https://doi.org/10.1109/TIM.2013.2255993.

[4] S. Das, N. Jain, A. Saha, Noncontact self-vibration compensated position sensitive detector based low-frequency vibration measurement, IEEE Trans. Instrum. Meas. 73 (2024) 1–8, https://doi.org/10.1109/TIM.2024.3367381.

[5] M. Ozbek, F. Meng, D.J. Rixen, Challenges in testing and monitoring the in-operation vibration characteristics of wind turbines, Mech. Syst. Signal Process. 41 (1) (Dec. 2013) 649–666, https://doi.org/10.1016/j.ymssp.2013.07.023.

[6] M. Ozbek, D.J. Rixen, O. Erne, G. Sanow, Feasibility of monitoring large wind turbines using photogrammetry, Energy 35 (12) (2010) 4802–4811.

[7] T.J. Beberniss, D.A. Ehrhardt, High-speed 3D digital image correlation vibration measurement: recent advancements and noted limitations, Mech. Syst. Signal Process. 86 (Mar. 2017) 35–48, https://doi.org/10.1016/j.ymssp.2016.04.014.

[8] R. Wu, D. Zhang, Q. Yu, Y. Jiang, D. Arola, Health monitoring of wind turbine blades in operation using three-dimensional digital image correlation, Mech. Syst. Signal Process. 130 (Sep. 2019) 470–483, https://doi.org/10.1016/j.ymssp.2019.05.031.

[9] W. Wang, J. Yang, J. Dai, A. Chen, EEMD-based videogrammetry and vibration analysis method for rotating wind power blades, Measurement 207 (Feb. 2023) 112423, https://doi.org/10.1016/j.measurement.2022.112423.

[10] N.A. Valente, C.T. do Cabo, Z. Mao, C. Niezrecki, Quantification of phase-based magnified motion using image enhancement and optical flow techniques, Measurement 189 (Feb. 2022) 110508, https://doi.org/10.1016/j.measurement.2021.110508.

[11] N. Wadhwa, M. Rubinstein, F. Durand, W.T. Freeman, Phase-based video motion processing, ACM Trans. Graph. 32 (4) (Jul. 2013) 1–10, https://doi.org/10.1145/2461912.2461966.

[12] V. Saveljev, J.-Y. Son, H. Lee, G. Heo, Non-contact measurement of vibrations using deferred moiré patterns, Adv. Mech. Eng. 15 (4) (Apr. 2023) 16878132221143885, https://doi.org/10.1177/16878132221143885.

[13] *The Theory of the moiré phenomenon*, vol. 38, in: I. Amidror (Ed.), Computational Imaging and Vision, vol. 38, Springer, London, 2009, https://doi.org/10.1007/978-1-84882-181-1.

[14] S. Gruppetta, '2D Fourier transform in Python: Create any image using only sine functions', The Python Coding Book. Accessed: April. 22, 2024. [Online]. Available: https://thepythoncodingbook.com/2021/08/30/2d-fourier-transform-in-python-and-fourier-synthesis-of-images/.

[15] G. C. Larsen, M. H. Hansen, A. Baumgart, and I. Carlén, 'Modal Analysis of Wind Turbine Blades'.

Yi-Hsiang Liao, Lijuan Wang*, Yong Yan
*University of Kent, Canterbury, United Kingdom*

* Corresponding author.
*E-mail addresses:* yl370@kent.ac.uk (Y.-H. Liao), l.wang@kent.ac.uk (L. Wang), y.yan@kent.ac.uk (Y. Yan).